Available online at www.sciencedirect.com
SCIENCE DIRECT®
PERGAMON
International Journal of Mechanical Sciences 45 (2003) 851–871
International Journal of MECHANICAL SCIENCES
www.elsevier.com/locate/ijmecsci

The plastic collapse and energy absorption capacity of egg-box panels

Marc Zupan[a], C. Chen[b], N.A. Fleck[a,*]

[a] *Department of Engineering, University of Cambridge, Trumpington Street, Cambridge CB2 1PZ, UK*
[b] *The State Key Lab of Mechanical Structural Strength and Vibration, Xi'an Jiaotong University, Xi'an 710049, People's Republic of China*

Received 17 October 2002; received in revised form 29 May 2003; accepted 17 July 2003

Abstract

The plastic collapse response of aluminium egg-box panels subjected to out-of-plane compression has been measured and modelled. It is observed that the collapse strength and energy absorption are sensitive to the level of in-plane constraint, with collapse dictated either by plastic buckling or by a travelling plastic knuckle mechanism. Drop weight tests have been performed at speeds of up to 6 m s^{-1}, and an elevation in strength with impact velocity is noted. A 3D finite element shell model is needed in order to reproduce the observed behaviours. Additional calculations using an axisymmetric finite element model give the correct collapse modes but are less accurate than the more sophisticated 3D model. The finite element simulations suggest that the observed velocity dependence of strength is primarily due to strain-rate sensitivity of the aluminium sheet, with material inertia playing a negligible role. Finally, it is shown that the energy absorption capacity of the egg-box material is comparable to that of metallic foams.

Keywords: Egg-box material; Plastic buckling; Plastic collapse; Travelling knuckle; Energy absorption

1. Introduction

Energy absorbing materials find widespread application ranging from protective packaging of delicate components to crash mitigation in automobiles and aircraft. Existing energy absorbers include metal foams [1], honeycombs [2], and thin walled tubes [3–5]. There is, however, a need for low cost, lightweight alternatives, partly due to the demands of increased fuel efficiency and passenger safety. A potential new class of energy absorbing material is the egg-box panel, as shown in

* Corresponding author. Tel.: +44-1223-332-650; fax: +44-1223-332-662.
E-mail address: naf1@eng.cam.ac.uk (N.A. Fleck).

0020-7403/$ - see front matter © 2003 Elsevier Ltd. All rights reserved.
doi:10.1016/S0020-7403(03)00136-X

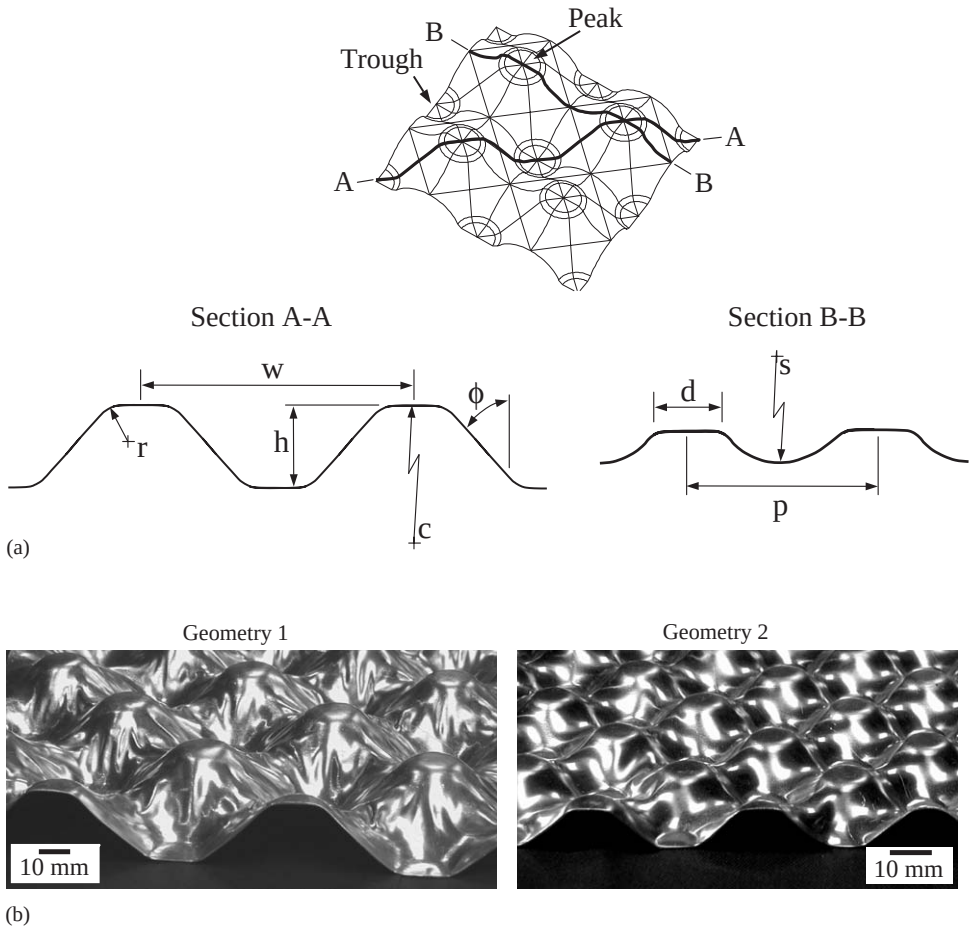

Fig. 1. (a) Sketch of the egg-box structure with section views; (b) Photographs of the aluminium egg-boxes, geometries 1 and 2. Pronounced wrinkling occurs during cold pressing of geometry 1.

Fig. 1: this can be cold or hot pressed to shape from metallic, polymeric and composite sheet. In this study, the collapse response is explored for egg-box panels made from Al 1050 H111 aluminium alloy.

Metallic energy absorbing structures dissipate work by the activation of stationary or moving plastic hinges, or by plastic stretch. For example, open-cell metallic foams absorb energy by the rotation of stationary hinges at cell edges. This collapse mode is inefficient from the viewpoint of structural mass: most of the material remains elastic during collapse, and only a small volume fraction deforms plastically. A much larger proportion of the structure experiences plastic dissipation for the case of *stretching microstructures* such as the axial crushing of tubes, octet-truss structures, and high density closed cell foams [4–8]. High-energy absorption is also achieved buy structures which deform by a *travelling plastic knuckle*. Examples include the inversion of a tube, cone or hemispherical shell [7,9–12], where the structure is inverted by the propagation of a narrow plastic toroidal region moving along its length. Plastic deformation in the travelling plastic knuckle is by a

combination of longitudinal bending and hoop stretching [13]. Preliminary experiments on egg-box material [14] suggest that egg-boxes deform by either the rotation of a stationary plastic hinge or by a travelling plastic knuckle, depending upon the in-plane kinematic constraints imposed upon the egg-box.

The scope of this paper is as follows. The through-thickness compressive strength of egg-box panels is measured for various choices of wall thickness, constraint, and loading-platen velocity (10^{-6}–6 m s^{-1}). The observed modes of collapse and associated load versus displacement responses are compared with finite element predictions; these calculations assume either a rotationally symmetric cone or a full 3D geometry. The source of the observed sensitivity of collapse response to the loading-platen velocity is explored numerically. Finally, the energy absorbing capacity of egg-box panels is compared with that of metallic foams.

2. The egg-box panel and the test method

2.1. Egg-box geometries and material properties

Egg-box panels of commercially pure, annealed 1050 H111 aluminium alloy were cold pressed between lubricated closed dies. Each panel was of dimension 300 mm × 300 mm in plan view, and comprised a set of truncated cones in an arrangement of four-fold in-plane symmetry, as sketched in Fig. 1a. Two different die sets were used in order to generate the two geometries listed in Table 1 and displayed in Fig. 1b; geometry 2 was approximately half the size of geometry 1. It is evident from the photographs shown in Fig. 1b that geometry 1 contains pronounced wrinkling in the as-pressed state; it is shown below that this imperfection leads to a reduction in compressive strength.

Define the relative density $\bar{\rho}$ of a panel as the mass of the panel divided by the mass of a solid block with the same enclosed volume. Then, a wide range of relative density $\bar{\rho} = 0.028$–0.092 was achieved for the two geometries by selecting wall thicknesses of the aluminium alloy sheet prior to cold-pressing in the range 0.34–0.80 mm. The wall thicknesses t and corresponding values of $\bar{\rho}$ are listed in Table 2.

The nominal tensile stress–strain response of the as-received Al 1050 H111 sheet was measured at a strain rate of 10^{-4} s^{-1} in accordance with the ASTM standard E8M-96 [15]. The results are presented in Fig. 2 for sheet thicknesses of 0.50 and 0.80 mm; egg-box panels of other wall thicknesses were obtained from the sheets of thickness 0.50 and 0.80 mm by phosphoric acid etching after pressing. It is clear from Fig. 2 that the 0.5 mm thick sheet is approximately 20% stronger than the 0.8 mm thick sheet, but both possess a high-tensile failure strain of approximately 0.45 (necessary for successful cold-pressing).

Table 1

	h (mm)	d (mm)	w (mm)	p (mm)	c (mm)	r (mm)	s (mm)	ϕ (deg)
Geometry 1	20	15	70	50	51	11	20	45
Geometry 2	10	9	35	25	51	4.4	11	48

Table 2

	Sheet thickness, t (mm)	Relative density, $\bar{\rho}$
Geometry 1	0.50	0.028
	0.65	0.035
	0.80	0.044
Geometry 2	0.34	0.039
	0.50	0.054
	0.80	0.092

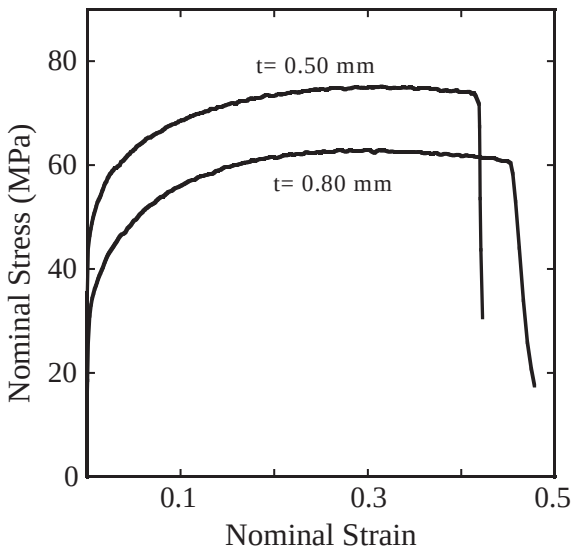

Fig. 2. Measured uniaxial tensile stress–strain curves for the as-received 1050 H111 aluminium alloy sheets of thickness $t = 0.50$ and 0.80 mm.

Vickers micro-hardness tests were used to determine the degree of strain hardening due to cold pressing of the Al sheet. A hardness traverse at selected locations of the as-pressed egg-box gave hardness values in the narrow range of HV = 224–233 and 185–200 MPa for sheets of original thickness 0.5 and 0.8 mm, respectively. These values of hardness are approximately 19% above the measured hardness of the annealed sheets prior to cold pressing.

2.2. Compression tests on panels

Specimens of square shape in plan view were cut from the as-pressed panels to a dimension of 5×5 unit cells. Compression tests were performed in the through-thickness direction of the panels, and these are hereafter referred to as *transverse-compression* tests. The effect of velocity of loading-platen was explored using a screw-driven test machine of load capacity 25 kN (velocity

$=10^{-6}$–10^{-2} m s^{-1}). Dynamic experiments at speeds of up to 6 m s^{-1} were conducted using a drop-weight tower with a loading mass of 5.5 kg. The load was measured with a 100 kN Kistler[1] load cell, and a 1 kHz low pass filter was used to reduce load cell ringing. The relative displacement of loading platens was measured by a laser extensometer in the low speed tests, and by a high bandwidth linear potentiometer[2] in the drop weight tests; the load and displacement histories in the drop weight tests were verified through use of an accelerometer fitted to the dropped mass.

Three types of lateral constraint were imposed on the specimens:

(i) *Unconstrained*: The egg-box panel was placed between unlubricated loading-platens.
(ii) *Bonded*: The panel was adhered to 2 mm thick 2024-T3 aluminium alloy face sheets using polyurethane adhesive (Vantico XB5090-1/XB5304).
(iii) *Constrained*: The panel was placed in a hollow box of adjustable square cross-section, to impose zero in-plane strain.

The imposed constraints were chosen in order to simulate potential applications of the panels as follows. The unconstrained response is representative of a high stack of unbonded panels, as explored in Ref. [14]; the bonded panels provide the expected sandwich panel response, and the constrained tests give the response for a wide panel undergoing negligible in-plane strain. A preliminary set of experiments was conducted in order to determine the size of egg-box specimen to give a response, which is representative of that for a large panel. It was found that a specimen of dimension 5×5 unit cells was adequate for the bonded and constrained cases. However, in the unconstrained case, the presence of friction between the loading platens and specimen gave rise to some constraint against collapse: consequently, the nominal stress–strain curve for transverse-compression increased monotonically with increasing specimen size. For the sake of simplicity, results for unconstrained specimens will are given only for 5×5 unit cells.

2.3. Measured collapse response of egg-box panels at low velocity

The effect of relative density and constraint upon the transverse-compression response is shown in Fig. 3 for geometry 1 and in Fig. 4 for geometry 2. Here and below, the nominal stress $\bar{\sigma}$ and strain $\bar{\varepsilon}$ for the egg-box structure are defined in the through-thickness direction, with the egg-box panel treated as a homogenised effective medium. The imposed crushing velocity was 2×10^{-6} m s^{-1} for geometry 1 and 1×10^{-6} m s^{-1} for geometry 2, in order to give an average compressive strain rate of 1×10^{-4} s^{-1} over the height of the egg-box material. With the exception of the bonded tests of geometry 1, the experimental scatter in response is negligible and the single curves shown in Figs. 3 and 4 are representative of behaviour. For the bonded sandwich panels of geometry 1, six repeat tests were performed at each relative density, and the extremes of behaviour are plotted in Fig. 3. The scatter in the bonded-panel response of geometry 1 is attributed to the presence of the wrinkling imperfections.

Overall, a consistent picture emerges for each choice of loading constraint: as the relative density increases the qualitative response is unchanged but the stress level increases. Insight into the operative

[1] Kistler Instrumentation Corp., Amherst, NY, USA.
[2] Techni Measure Sensors, Studley, Warwickshire, UK.

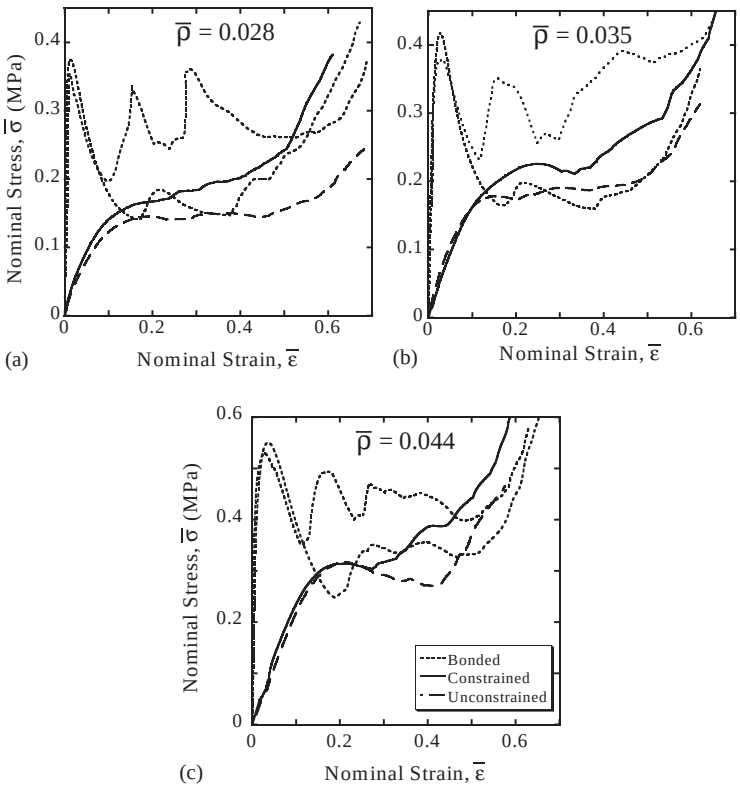

Fig. 3. Through-thickness collapse response of the geometry 1 egg-box panel for the relative densities: (a) $\bar{\rho} = 0.028$; (b) $\bar{\rho}=0.035$; (c) $\bar{\rho}=0.044$. In each plot, representative nominal stress–strain curves are given for constrained and unconstrained through-thickness compression of the egg-box structure. The extremes of behaviour are shown for the bonded case by a pair of curves.

plastic collapse modes for each constraint condition was obtained by interrupting the tests and by sectioning and polishing the cross-section of the core. Typical sections and the associated collapse curves are shown in Fig. 5 for geometry 2; we consider each constraint case in turn.

(i) *Unconstrained test*: The macroscopic compressive stress versus strain curve shows an initial nonlinear response associated with plastic yield of the core. The egg-box geometry contains a slight crown and longitudinally curved (rather than perfectly straight) side-walls: these induce elastic–plastic bending at low load levels. A peak strength is obtained at a nominal compressive strain of approximately 0.1, and is associated with the plastic snap-through of the crown and buckling of the side-walls (labelled point 2 on the collapse response and in the montage of photographs). A load drop is observed with the continued activation of this buckling mode, point 3. In the final stage (in the vicinity of point 4), the side-walls of the core come into contact with the loading platens, and this results in a steeply rising stress versus strain response. This is termed densification.

The shape of the collapse curve for the unconstrained specimens has some sensitivity to the magnitude of $\bar{\rho}$, see Figs. 3 and 4. At sufficiently low relative densities, $\bar{\rho} < 0.039$, a plateau in stress accompanies plastic buckling, while at higher values of $\bar{\rho}$, a load drop emerges after buckling.

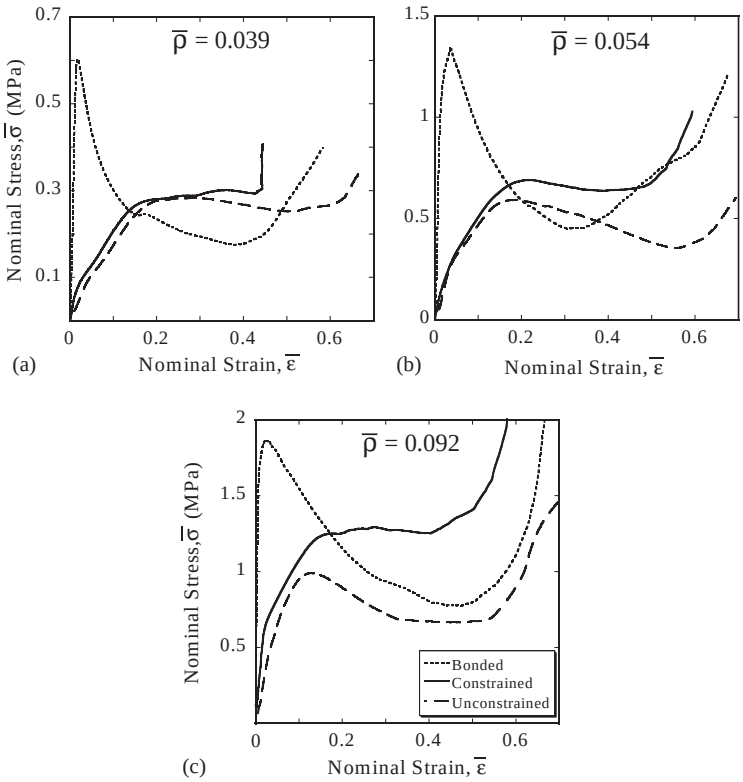

Fig. 4. Through-thickness collapse response of geometry 2 egg-box for the relative densities: (a) $\bar{\rho} = 0.039$; (b) $\bar{\rho} = 0.054$; (c) $\bar{\rho} = 0.092$. In each plot, representative nominal stress–strain curves are given for bonded, constrained and unconstrained compression.

(ii) *Bonded test*: The effect of bonding the crowns of the egg-box to the face sheets is to stiffen and strengthen the sandwich panel response, see Figs. 3 and 4. A comparison of the sections shown in Figs. 5a and b reveals that plastic collapse is again by the buckling of the side-walls of the core. However, the bonding inhibits pre-buckling deformation of the spherical crowns (stages 1–2), and prevents snap-through. Consequently, plastic buckling of the side-walls is delayed and the peak strength is increased. At large compressive nominal strains on the order of 0.5, the core has crushed to a final state of densification (as illustrated by point 4). There is however a complication to the response exhibited by geometry 1, see Fig. 3. The macroscopic compressive stress versus strain curve displays oscillations in the plastic buckling regime; examination of the deformed core (Fig. 6) reveals that these oscillations are associated with short wavelength longitudinal buckling of the side walls. The buckling pattern is reminiscent of concertina buckling in the axial crushing of a tube [3,4], and initiates adjacent to the crowns of the egg-box.

(iii) *Constrained test*: Fig. 5c shows the representative behaviour for geometry 2, with full lateral constraint imposed and the face sheets absent. The initial response is slightly stiffer and stronger than that of the unconstrained specimens, and the responses diverge at nominal strain levels exceeding about 0.2. In the constrained case, plastic collapse occurs at almost constant load (Figs. 3 and 4),

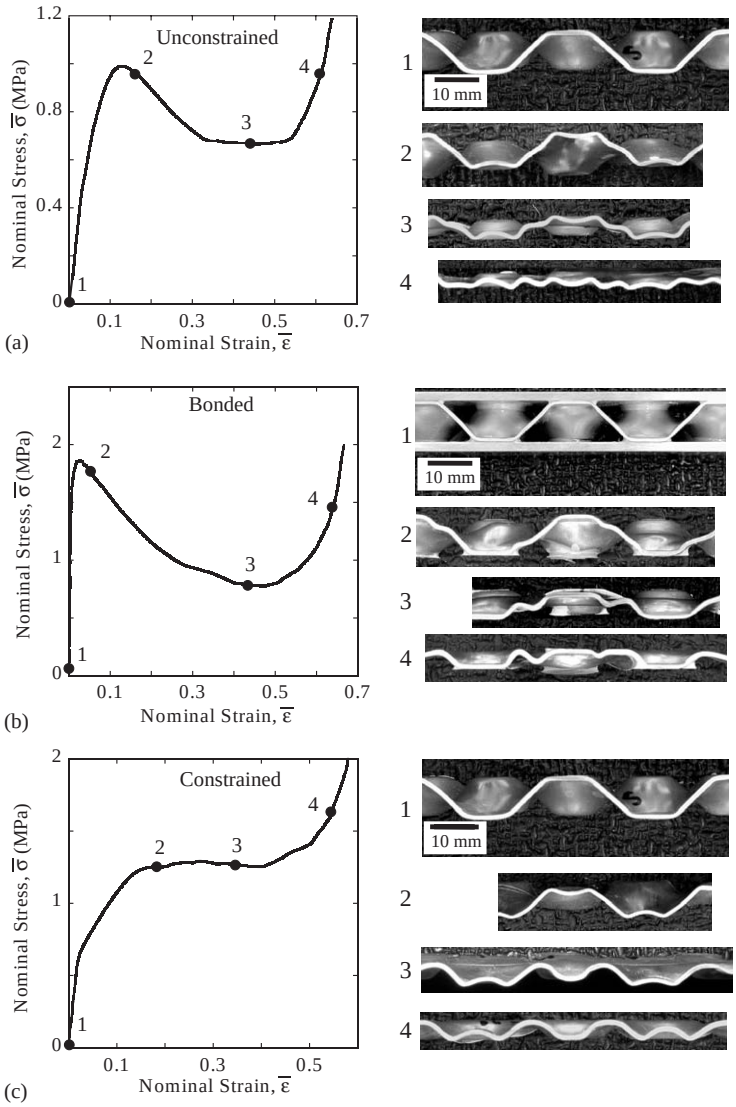

Fig. 5. The collapse response of geometry 2 egg-box and $\bar{\rho} = 0.092$ for (a) unconstrained, (b) bonded and (c) constrained loading. In each case, the profile at selected stages of deformation is shown by photographs taken from multiple interrupted tests.

and is associated with the formation of a travelling plastic knuckle from each crown, see Fig. 5c. The travelling plastic knuckle comprises a ring-shaped plastic hinge and leads to the progressive inversion of the conical side-wall of each unit cell. This travelling knuckle phenomenon is qualitatively similar to that observed in the inversion of a hemispherical shell [10–12]. Densification ensues at a nominal compressive strain of the order of 0.5.

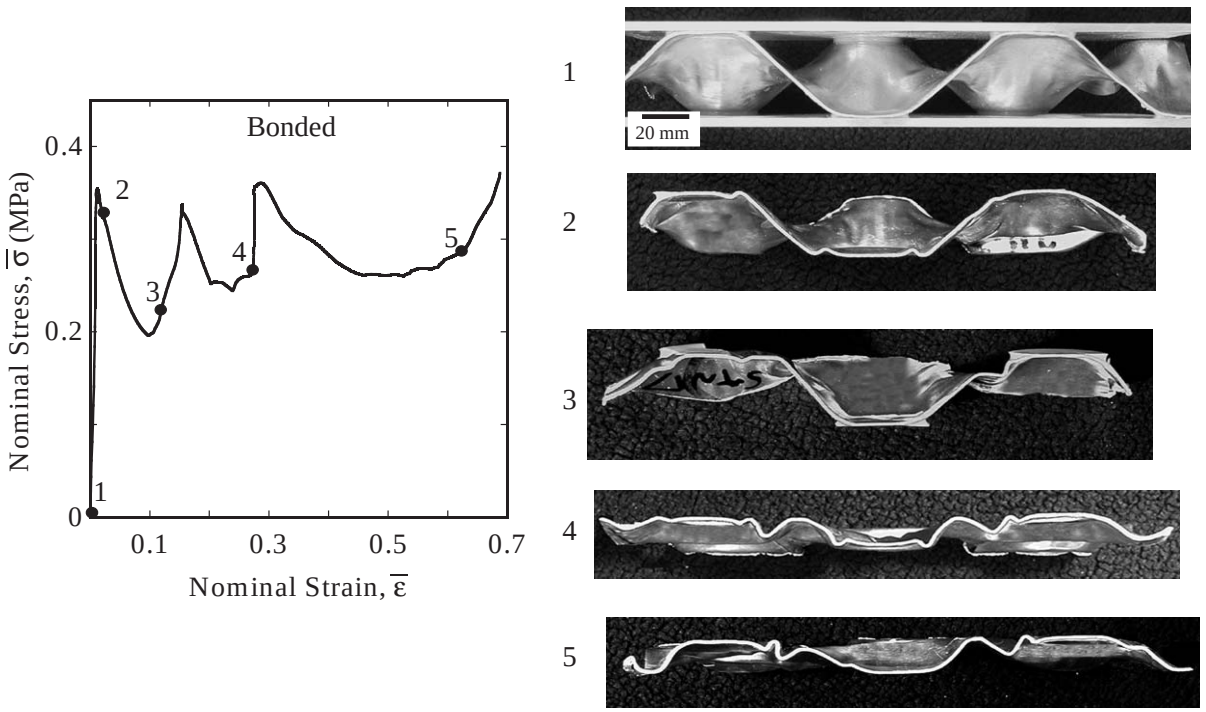

Fig. 6. The collapse response for the bonded egg-box of geometry 1 and $\bar{\rho} = 0.028$. The profiles at selected stages of deformation are shown by photographs taken from multiple interrupted tests.

2.4. Effect of loading speed upon collapse response

The effect of the loading platen speed upon the collapse response for the constrained and bonded panels of geometry 2 has been explored for a relative density of 0.092. The responses are shown in Fig. 7a for bonded sandwich panels and in Fig. 7b for constrained panels. (It is less likely that unconstrained panels will find practical application, and so no drop weight tests were performed on the unconstrained panels.) Measurements of the displacement versus time and acceleration versus time, histories during the drop weight experiments confirmed that the change in drop weight velocity over the duration of the test could be neglected. The change in velocity was greatest for experiments on bonded egg-box samples of high relative density ($\bar{\rho} = 0.092$), and for such tests the velocity decreased from 6 to 5.1 m s^{-1} over the test. Thus the initial velocity of the drop weight sets the strain rate at the peak load.

It is believed that the scatter in initial elastic slope is associated with misalignment of the loading platens, particularly in the drop weight machine. Upon taking Figs. 7a and b together, it is clear that the strength of the bonded and constrained panels increases with loading-platen velocity: the peak strength at 6 m s^{-1} is approximately 20% higher than that at 0.01 m s^{-1}. A dynamic finite element simulation including material inertia and using a rate dependent constitutive model are reported below in order to determine whether the sensitivity of strength to impact velocity is due to material inertia or to material strain rate sensitivity.

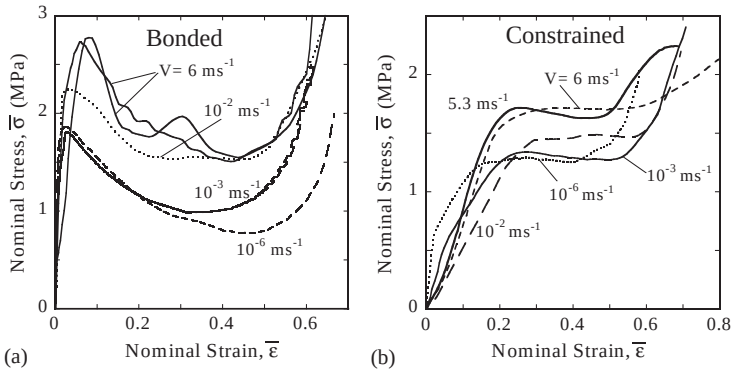

Fig. 7. Effect of the loading-platen velocity upon the observed nominal stress–strain behaviour of the Geometry 2 egg-box at $\bar{\rho} = 0.092$. (a) Bonded test; (b) constrained test.

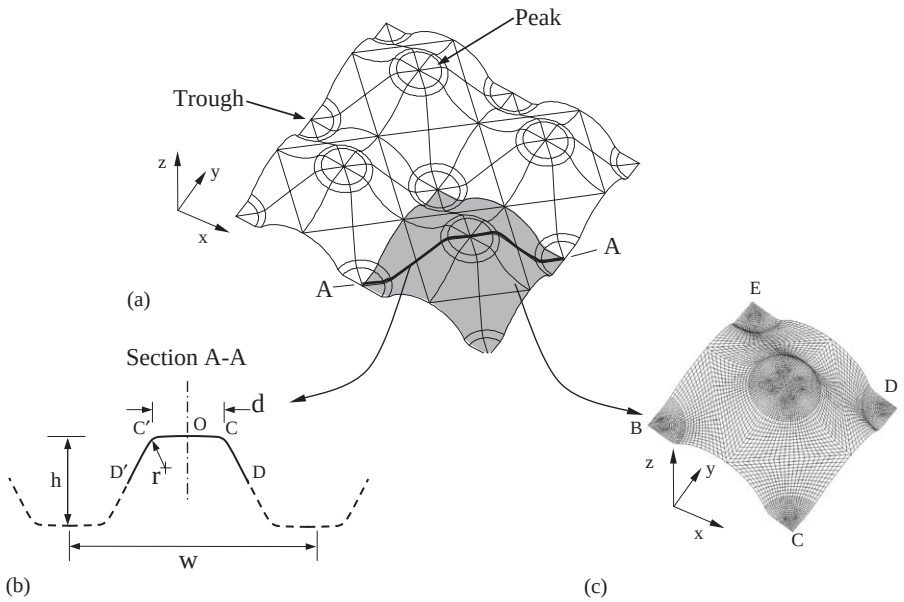

Fig. 8. Geometry of the finite element models: (a) parent geometry; (b) axisymmetric shell model; (c) 3D shell model.

3. Finite element simulations

The finite element method was used to simulate the plastic collapse of both egg-box geometries 1 and 2. For each geometry the egg-box was represented by a periodic 3D shell model (Fig. 8c), and by a much simpler axisymmetric shell model (Fig. 8b). Both types of finite element model were given the physical dimensions of Table 1 in order to allow for a direct comparison with experiment. Unless otherwise stated, the annealed Al 1050 H111 aluminium alloy was modelled by isotropic von Mises plasticity theory, with the uniaxial tensile response given by the stress–strain curves of Fig. 2.

The calculations were performed using the commercial finite element code ABAQUS Standard[3]. In each of the simulations the loading produced bending of the shell walls and no bifurcation instability was observed; thus, it was unnecessary to introduce an artificial imperfection to produce the buckling pattern.

The imposed boundary conditions in the finite element simulations are as follows. For unconstrained and constrained compression of the egg-box, the loading platens are represented by rigid, frictionless flat surfaces. In unconstrained compression, the periphery of the egg-box panel is free to expand laterally. Lateral expansion of the periphery is prevented in constrained compression. In the case of bonded compression, the egg-box core is taken to be perfectly adhered to rigid face sheets. To capture the peak load for the bonded core, it was necessary to pay particular attention to the bonded area between the core and face sheets: the bonded area extended beyond the egg-box crowns, as shown in the photographs of Fig. 5b.

3.1. Axisymmetric shell model

Although the egg-box panel is a 3D shell with four-fold in-plane symmetry, it was idealised by an axisymmetric conical frustum with flat tops, as shown by the section A–A of Figs. 8a and b. The frustums in Fig. 8b are defined by the diameter of circular top d, the wavelength between adjacent crowns w, the height of the egg-box h, and the fillet radius r. 3-noded axisymmetric shell elements (element type SAX2) are used to discretise the cone of section 'O–C–D', with appropriate boundary conditions imposed at the boundary nodes: the vertical displacement of node 'D' is fixed to prevent rigid body motion and; the radial displacement of node 'O' is also fixed. The radial displacement of node 'D' for the unconstrained case is free of motion, and is fixed for the bonded and constrained cases; details on the loading conditions are given below in Section 3.3. The anti-symmetry of the geometry with respect the mid-height plane implies no bending moment at node 'D', see Fig. 8b.

3.2. 3D shell model

The 3D model is based directly on the shaded area of the parent geometry in Fig. 8a. A typical mesh for the unit cell is shown in Fig. 8c with the coordinate system (x, y, z) marked. The egg-box panel is discretised by 4-noded finite strain shell elements (element type S4 in ABAQUS). Appropriate periodic boundary conditions on the translational displacement components were applied to the periphery of the unit cell 'B–C–D–E–B': zero in-plane average stress resultants to represent the unconstrained geometry, and zero in-plane strain averaged over the unit cell for the constrained case. The periodic boundary conditions used here are similar to those employed by Chen et al. [16] to investigate the elastic plastic yielding of 2D foams. Moreover, the symmetry requirements on the cross-section rotation on opposing boundaries of the unit cell gives none zero bending moment at the boundary. The nodal rotation is periodic from one unit cell to the next, and so the magnitude of the rotation is equal at opposing boundary nodes across the unit cell; similarly the bending moment at opposing nodes is identical. A mesh sensitivity study shows that the mesh given in Fig. 8c with 32 000 nodes and 24 000 elements provides adequate accuracy (within 1% of the collapse response).

[3] ABAQUS Standard User's Manual, Version 5.8, 2000. Hibbitt, Karlsson and Sorensen, Inc., Providence, RI.

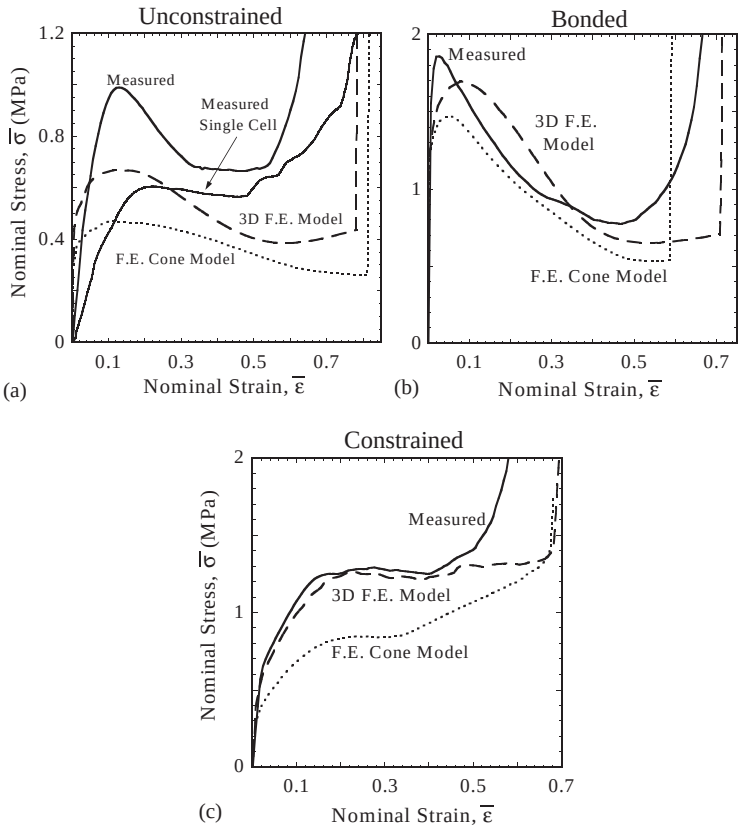

Fig. 9. Comparison of the measured and predicted collapse responses of the geometry 2 egg-box, for $\bar{\rho} = 0.092$: (a) unconstrained; (b) bonded; (c) constrained compression.

3.3. Quasi-static finite element results

The axisymmetric and 3D models were used to simulate the collapse of the egg-box. A comparison of the predicted and observed collapse response for the three types of constraint is given in Fig. 9 for geometry 2, with wall thickness $t = 0.80$ mm and $\bar{\rho} = 0.092$. In order to gain additional insight into the collapse modes, the mesh at selected stages of overall deformation is shown in Fig. 10 for the axisymmetric model, and in Fig. 11 for the 3D model (only $\frac{1}{8}$th of the 3D mesh is shown for clarity, as the predicted buckling mode shared the symmetry of the initial geometry). The quality of agreement between predicted and observed response is representative of that for other relative densities and for geometry 1, and additional comparisons are omitted for the sake of brevity. As a general remark, the finite element cone model gives a consistently lower strength than the 3D model. In part, this is due to the different boundary conditions imposed. In the cone model vanishing bending moments are assumed at the periphery of the model (point D in Fig. 8b). In contrast, periodic nonvanishing moments exist at the periphery of the 3D finite element model as discussed in Section 3.2. In the following, we consider each loading condition in turn.

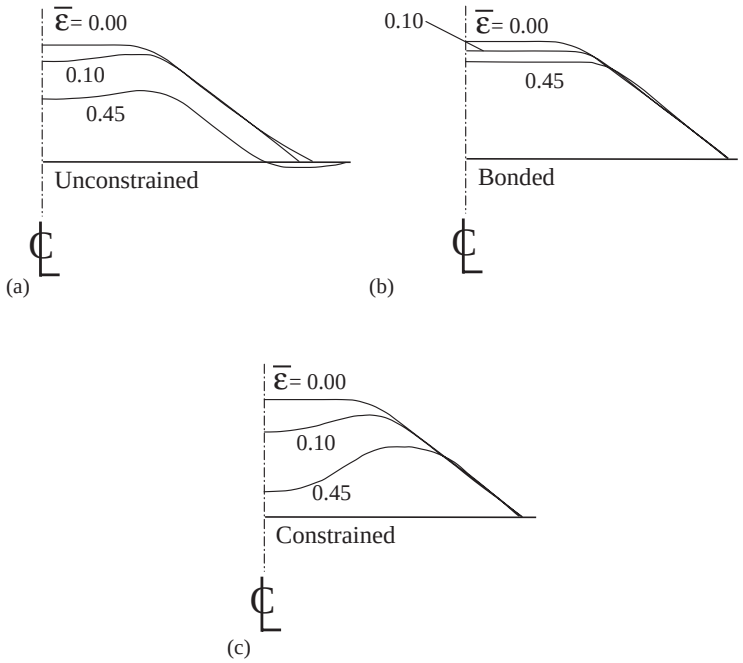

Fig. 10. The predicted deformation of the egg-box by the axisymmetric model at selected values of nominal strain $\bar{\varepsilon}$. Geometry 2, $\bar{\rho} = 0.092$: (a) unconstrained compression; (b) bonded compression; (c) constrained compression.

(i) *Unconstrained egg-box*: The axisymmetric and 3D models both collapsed by plastic buckling with a deflected shape similar to that observed, compare Figs. 10a, 11a and 5a. It is seen from Fig. 9a that both the 3D and axisymmetric shell models considerably underestimate the measured collapse response for the egg-box with 5×5 unit cells. It is argued that friction exists between the platens and the crowns of the egg-box; consequently, lateral expansion of the egg-box is restrained, and the measured buckling load is elevated. To confirm this, the measured collapse response for a single-cell egg-box is included in Fig. 9a; it is clear that the measured response is sensitive to the number of unit cells composing the specimen. The finite element analyses for the unconstrained case were performed for frictionless compression, and are in good agreement with the measured behaviour of the specimen containing a single cell, see Fig. 9a.

It is anticipated that specimens containing a large number of unit cells will behave similarly to the constrained specimens: the presence of sliding friction at the crowns of the 'unconstrained specimens' will lead to an increased lateral constraint with increasing aspect ratio of specimen. Thus, it is expected that the collapse mode of the 'unconstrained specimens' will switch from plastic buckling to the travelling knuckle mechanism when the aspect ratio exceeds a critical value.

(ii) *Sandwich with bonded egg-box core*: The 3D model reproduces the observed collapse response, Fig. 9b, and the observed deformation mode; compare Figs. 10b and 11b with 5b. In contrast, the axisymmetric shell model slightly under-predicts the collapse behaviour, and approximately

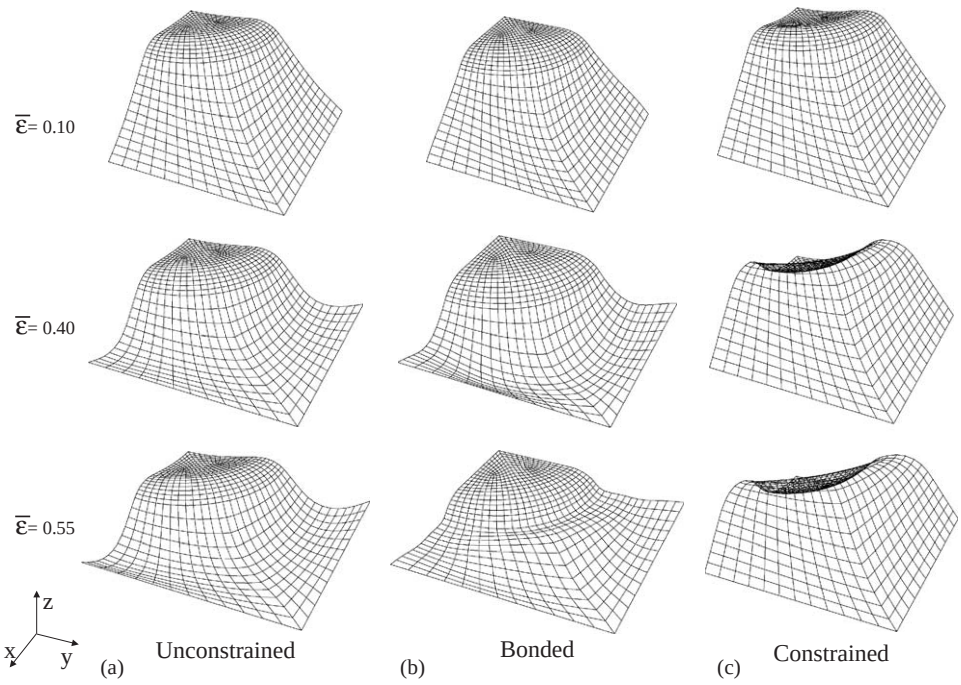

Fig. 11. The predicted deformation of the egg-box by the 3D model at selected values of nominal strain $\bar{\varepsilon}$. Geometry 2, $\bar{\rho} = 0.092$: (a) unconstrained compression; (b) bonded compression; (c) constrained compression.

captures the observed mode of deformation, see Fig. 9b. The precise value of predicted peak load is sensitive to the assumed area of bonding between crown of egg-box and face-sheet.

(iii) *Constrained egg-box*: The observed collapse mode of a travelling plastic knuckle (Fig. 5c) is confirmed by both the 3D and axisymmetric models, Figs. 10c and 11c. During the phase of plastic knuckle propagation the load is almost constant, refer to Fig. 9c. However, the axisymmetric model under-predicts the collapse load by approximately 30%. It is concluded that the assumption of an axisymmetric geometry leads to an under-prediction in strength.

3.4. Dependence of collapse response upon the relative density of egg-box

The egg-box can be treated as an effective medium, endowed with an *effective Young's modulus* $\bar{E}$ in the height-direction, an *effective yield strength* $\bar{\sigma}_y$ set by the peak stress at the onset of plastic buckling (unconstrained and bonded cases) or by the plateau stress for plastic knuckle propagation (constrained case), and an *energy per unit enclosed volume* W_V defined by the area under the nominal stress–strain curve to the densification point, taken at a nominal strain of 0.5. Although this definition of densification is arbitrary, the value of W_V is found to be insensitive to the assumed stress level at densification.

The measured values of $\bar{E}$, $\bar{\sigma}_y$ and W_V for the bonded and constrained egg-box cores are plotted as discrete data points against the relative density $\bar{\rho}$ in Figs. 12–14, respectively. These figures include the 3D finite element predictions: solid lines are shown for geometry 1 and dotted lines for geometry 2.

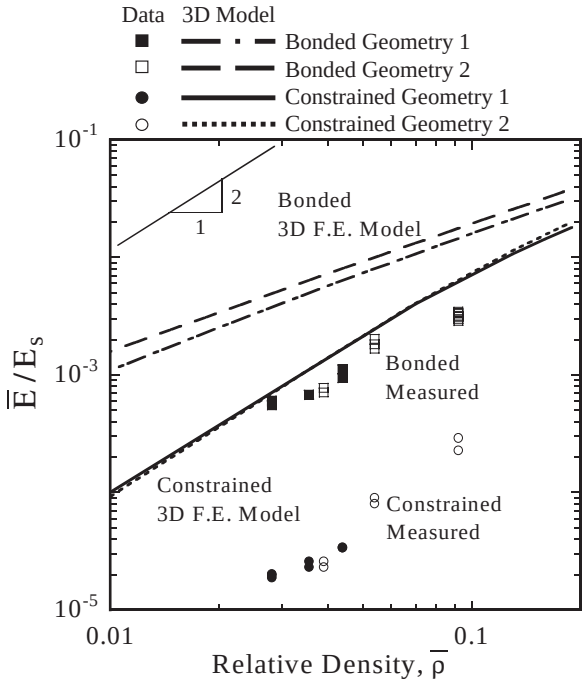

Fig. 12. Measured and predicted normalised effective Young's modulus $\bar{E}/E_s$ of constrained and bonded egg-box versus relative density $\bar{\rho}$.

Consider first the effect of relative density $\bar{\rho}$ upon $\bar{E}$. It is clear from Fig. 12 that the measured $\bar{E}$ scales with $\bar{\rho}$ according to

$$\frac{\bar{E}}{E_s} = 0.4\bar{\rho}^2 \quad \text{for bonded core} \tag{1}$$

and

$$\frac{\bar{E}}{E_s} = 0.03\bar{\rho}^2 \quad \text{for constrained core,} \tag{2}$$

where $E_s = 70$ GPa is Young's modulus of the solid aluminium alloy sheet. The functional form of this dependence suggests that the effective modulus is controlled by elastic bending of the egg-box structure, as noted previously for metal foams [1]. It is striking that the predicted modulus is nearly an order of magnitude greater than the measured value, for both the constrained and bonded egg-boxes. This discrepancy is due to the local geometry of the crowns of the egg-box: elastic spring-back after cold-pressing of the egg-boxes produces crowns which were not flat-topped but have spherical caps of small but finite curvature. Numerical experiments confirm that the stiffness of the egg-box is sensitive to the crown curvature. For example, the assumption of a spherical cap of height equal to the sheet thickness t gives rise to a drop in $\bar{E}$ by an order of magnitude.

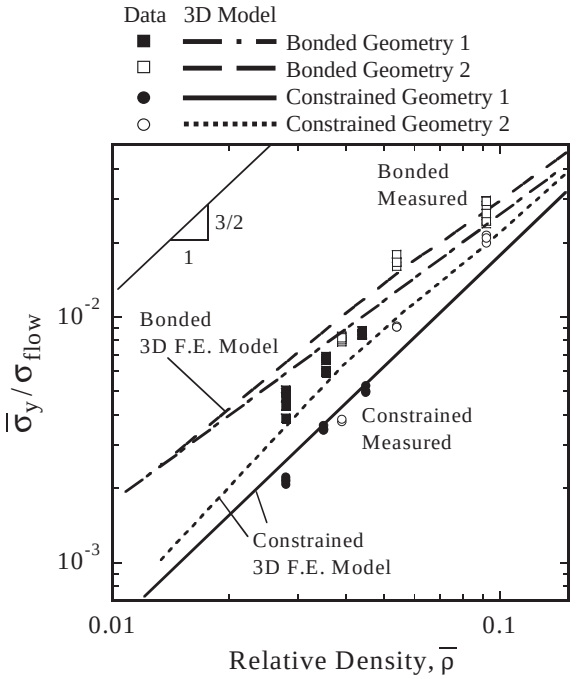

Fig. 13. Measured and predicted normalised yield strength $\bar{\sigma}_y/\sigma_{flow}$ of constrained and bonded egg-box versus relative density $\bar{\rho}$.

Next, consider the dependence of the *effective yield strength* $\bar{\sigma}_y$ upon $\bar{\rho}$, as shown in Fig. 13. It is seen from Fig. 13 that the effective strength is approximated by the relations

$$\frac{\bar{\sigma}_y}{\sigma_{flow}} = 0.9\bar{\rho}^{3/2} \quad \text{for bonded core} \tag{3}$$

and

$$\frac{\bar{\sigma}_y}{\sigma_{flow}} = 0.5\bar{\rho}^{3/2}, \quad \text{for constrained core,} \tag{4}$$

where σ_{flow} is the plastic flow stress of the solid aluminium sheet defined as the average of the ultimate tensile strength and the yield stress. It is known from previous studies on metallic foams that an exponent of $\frac{3}{2}$ is expected when the strength is dictated by plastic bending of the microstructure [1,8]. Since the strength of metal foams is given by [1,8],

$$\frac{\bar{\sigma}_y}{\sigma_{flow}} = 0.3\bar{\rho}^{3/2}, \tag{5}$$

it is concluded that the performance of egg-box panels exceeds that of metal foams.

A plot of *energy per unit enclosed volume* W_V versus $\bar{\rho}$ is given in Fig. 14. The data suggest the correlations

$$\frac{W_V}{\sigma_{flow}} = 0.3\bar{\rho}^{3/2} \quad \text{for bonded core} \tag{6}$$

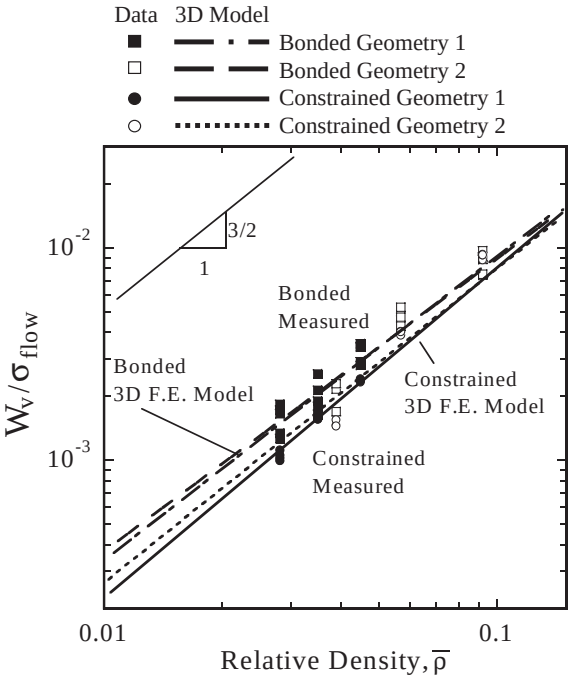

Fig. 14. Measured and predicted normalised energy absorption per unit volume W_V/σ_{flow} of constrained and bonded egg-box versus relative density $\bar{\rho}$.

and

$$\frac{W_V}{\sigma_{flow}} = 0.15\bar{\rho}^{3/2} \quad \text{for constrained core.} \tag{7}$$

3.5. Role of material inertia and rate sensitivity

The observed collapse response of the bonded and constrained egg-box structures are mildly sensitive to the loading platen velocity, recall Fig. 7. To explore the relative role of material inertia and material strain rate sensitivity, the finite element predictions for the quasi-static, rate insensitive solid were augmented by a dynamic finite element study, again using ABAQUS standard. 3D simulations were performed for geometry 2 at a relative density $\bar{\rho} = 0.092$. In the simulations, the loading speed was held fixed in order to reflect the experimental condition that the deceleration of the drop weight anvil is negligible during each test. The same mesh (and boundary conditions) were used as for the quasi-static analysis, and the following two isotropic constitutive descriptions were adopted:

(i) the rate independent elastic–plastic behaviour detailed above, and
(ii) an elastic–viscoplastic description, with a von Mises flow potential.

Rate dependence was implemented by assuming the von Mises stress is a function of the instantaneous von Mises strain rate, and of the accumulated von Mises strain. The functional dependence was

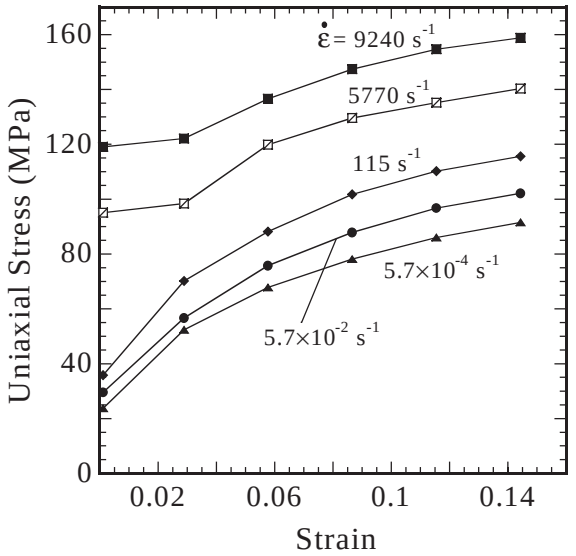

Fig. 15. The dynamic stress versus strain response of a commercially pure aluminium at selected strain rates, taken from Dowling et al. [17].

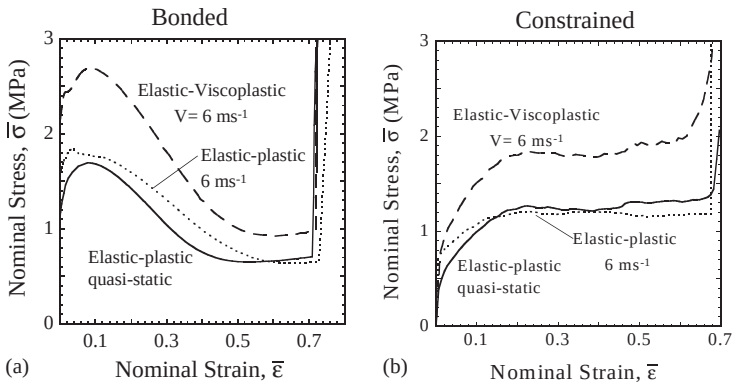

Fig. 16. Dynamic and quasi-static 3D simulation of the collapse response of (a) bonded and (b) constrained egg-box. Geometry 2, $\bar{\rho} = 0.092$.

programmed into the finite element analysis using a look-up table and linear interpolation complying with the format required by ABAQUS. Measured stress versus strain response of a commercially pure Al over a wide range of strain rates is taken from the study of Dowling et al. [17] and is presented in Fig. 15.

Finite element predictions for the bonded and constrained egg-box subjected to a fixed platen velocity of $V = 6\ \mathrm{m\ s^{-1}}$ are shown in Fig. 16a and b, respectively. It is emphasised that neither inertia nor strain rate effects are taken into account in the quasi-static simulations; only inertia effects are included in the dynamic elastic–plastic analysis whilst both inertia and strain rate sensitivity

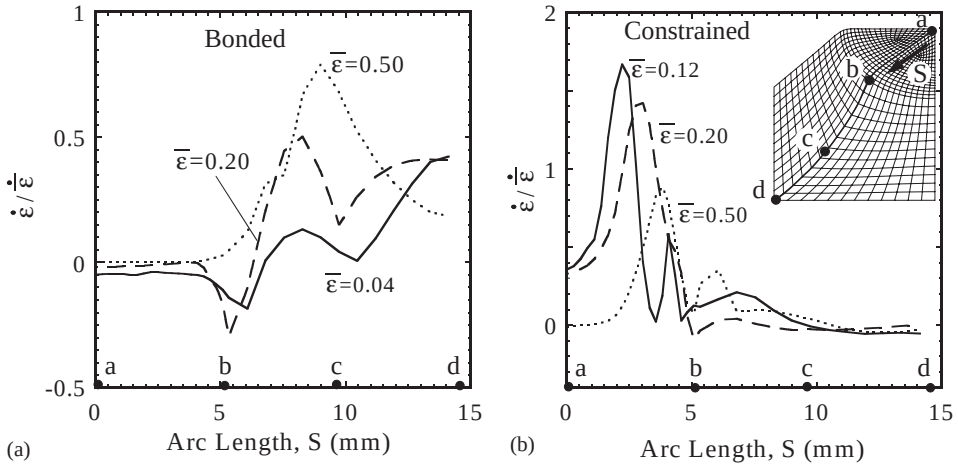

Fig. 17. Predicted maximum principal strain rate $\dot{\varepsilon}$ along the profile *a–b–c–d* of the egg-box structure, for a platen velocity of 6 m s^{-1}. Results are given at selected nominal through-thickness strains $\bar{\varepsilon}$ for (a) bonded and (b) constrained egg-box. The rate dependent constitutive description is employed. Geometry 2, $\bar{\rho} = 0.092$.

are included in the dynamic elastic–viscoplastic simulations. The dynamic elastic–plastic analysis predicts a negligible increase in strength above the quasi-static solution for egg-box loaded at a velocity $V = 6$ m s^{-1}; in contrast, the assumption of strain rate sensitivity gives an elevated peak strength comparable in magnitude to the observed value, cf. Figs. 16 with 7. We conclude that the observed sensitivity of collapse response to platen velocity is due to material strain rate sensitivity rather than to structural inertia.

It is instructive to plot the local strain rate distribution within the bonded and constrained egg-boxes as predicted by the dynamic, strain rate sensitive finite element model. Fig. 17 shows the maximum principal strain rate ($\dot{\varepsilon}$) along the profile *a–b–c–d* of the egg-box as defined in the inset of Fig. 17b. Results are given at selected values of nominal through-thickness strain of the egg-box $\bar{\varepsilon}$, and have been normalised by the nominal strain rate $\dot{\bar{\varepsilon}}$; note that a loading velocity of 6 m s^{-1} is equivalent to a nominal strain rate $\dot{\bar{\varepsilon}}$ of 600 s^{-1} for the egg-box of geometry 2.

It is noted from Fig. 17 that the local strain rate is non-uniform spatially, with clear evidence of a travelling plastic knuckle for the case of the constrained egg-box. The maximum value of the local strain rate is comparable in magnitude to the nominal through-thickness strain rate $\dot{\bar{\varepsilon}}$, giving local peak values of approximately 10^3 s^{-1}. This level of strain rate will give rise to only a moderate strain rate sensitivity [17].

4. Energy absorption

The energy absorption capacity of egg-box material (at a quasi static loading rate) is compared to that of metal foams in Fig. 18. Both the energy per unit initial volume W_V (Fig. 18a) and energy per unit mass $W_M \equiv W_V/\bar{\rho}\rho_S$ (Fig. 18b) are shown against the nominal yield strength $\bar{\sigma}_y$. Here, ρ_S is the density of the solid aluminium alloy. Note that the magnitude of $\bar{\sigma}_y$ dictates the level of

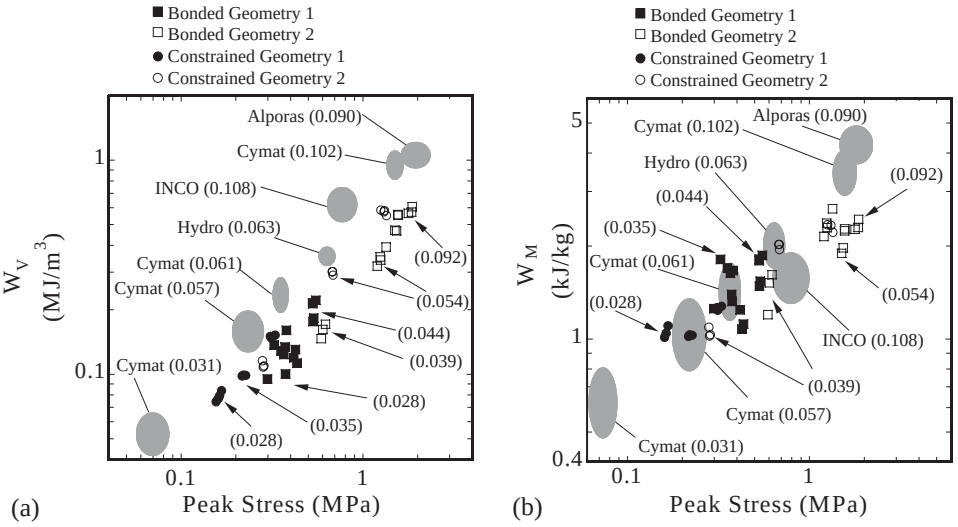

Fig. 18. Comparison of energy absorption for egg-box material and metallic foams. (a) Energy absorption per unit volume W_V versus the effective yield strength $\bar{\sigma}_y$ and (b) energy absorption per unit mass W_M versus $\bar{\sigma}_y$. The data are labelled by representative relative densities.

acceleration and deceleration of the protected component. For both bonded and constrained egg-boxes of geometries 1 and 2 it is clear from Fig. 18 (and from the relations 3,4,6 and 7) that

$$W_V = 0.3\bar{\sigma}_y. \tag{8}$$

Recall that the pre-factor gives a measure of the efficiency of the energy absorbing material: a value of unity denotes an ideal energy absorber, which fully crushes to a nominal strain of unity at constant stress. The metallic foams display the characteristic

$$W_V = 0.6\bar{\sigma}_y \tag{9}$$

and thereby surpass the energy absorption capacity of egg-box on the basis of efficiency. However, on the basis of energy absorption per unit mass W_M, egg-boxes and metallic foams are comparable in energy absorption capacity, see Fig. 18b.

5. Concluding remarks

The plastic collapse behaviour of egg-box panels has been investigated for unconstrained, bonded and constrained uniaxial compression. An axisymmetric shell model and a 3D shell model have been developed to simulate the observed collapse response and deformation mode. The 3D model is more accurate, but at the cost of greater complexity. The functional dependence of collapse strength upon relative density, and direct examination of the observed (and predicted) deformation modes suggest that collapse is dominated by bending of the side-walls of the egg-box. The velocity sensitivity noted in drop-weight tests is mild, and is due to the strain rate sensitivity of the aluminium alloy rather than to material inertia. A direct comparison with commercial metallic foams reveals that the

egg-box structure is a competing concept for energy absorption. Preliminary estimates suggest that the egg-box is also competitive with metallic foams on the basis of cost [18].

Acknowledgements

This work is supported by ONR through project 14-01-1-1051. The authors are grateful for helpful discussion with M.F. Ashby and V.S. Deshpande, and wish to thank Cellbond Composites Ltd, Huntingdon, UK for the provision of egg-box materials. CC would like to acknowledge the financial support of the Chinese Ministry of Education through Projects for Authors of National Excellent Ph.D. thesis (No. 200129). MZ would like to acknowledge the support of the National Science Foundation through the International Research Fellowship Program.

References

[1] Ashby MF, Evans AG, Fleck NA, Gibson LJ, Hutchinson JW, Wadley HNC. Metal foam: a design guide. Oxford: Butterworth Heinemann; 2000.
[2] Gibson LJ, Ashby MF. Cellular solids, structure and properties, 2nd ed. Cambridge: Cambridge University Press; 1997.
[3] Olivera J, Wierzbicki T. Crushing analysis of rotationally symmetric plastic shells. Journal of Strain Analysis 1982;17:229–36.
[4] Wierzbricki T, Abramowicz W. On the crushing mechanics of thin-walled structures. Journal of Applied Mechanics 1983;50:727–34.
[5] Mamalis AG, Manolakos DE, Saigal S, Viegelahn G, Johnson W. Extensible plastic collapse of thin-wall frusta as energy absorbers. International Journal of Mechanical Sciences 1986;28:219–26.
[6] Reddy TY, Reid SR. Phenomena associated with the crushing of metal tubes between rigid plates. International Journal of Solids and Structures 1980;16(6):545–62.
[7] Andrews KRF, England GL, Ghani E. Classification of the axial collapse of cylindrical tubes. International Journal of Mechanical Sciences 1983;25:687–96.
[8] Deshpande VS, Ashby MF, Fleck NA. Foam topology bending versus stretching dominant architectures. Acta Materialia 2001;49:1035–40.
[9] Al-Hassani STS, Johnson W, Lowe WT. Characteristics of inversion tubes under axial loading. Journal of Mechanical Engineering Science 1972;14(6):370–81.
[10] Calladine CR. Theory of shell structures. Cambridge: Cambridge University Press; 1983.
[11] Leckie FA, Penny RK. Plastic instability of spherical shell. In: Heyman J, Leckie FA, editors. Engineering plasticity. Cambridge: Cambridge University Press; 1968. p. 401–11.
[12] Updike DP. On the large deformation of a rigid plastic spherical shell compressed by a rigid plate. Journal of Engineering for Industry 1972;94:949–55.
[13] Deshpande VS, Fleck NA. Energy absorption of an egg-box material. Journal of the Mechanics and Physics of Solids 2003;51(1):187–208.
[14] Zupan M, Fleck NA, Ashby MF. The collapse and energy absorption of egg-box panels. In: Ghosh A, Snders T, Claar D, editors. Processing and properties of lightweight cellular metals and structures. Pennsylvania: TMS; 2002.
[15] ASTM Standard, E8M-96, Standard test methods of tension testing of metallic materials. Annual book of ASTM standards. ASTM, 1996.
[16] Chen C, Lu TJ, Fleck NA. Effect of imperfections on the yielding of two-dimensional foams. Journal of the Mechanics and Physics Solids 1999;47:2235–72.
[17] Dowling AR, Harding J, Campbell JD. Dynamic punching of metals. Journal of the Institute of Metals 1970; 98:215–24.
[18] Ashby MF. Cost estimation for sandwich cores. Private communication.